Hyperphosphatemia in chronic kidney disease exacerbates atherosclerosis via a mannosidases-mediated complex-type conversion of SCAP N-glycans

see commentary on page 1264

Chao Zhou[1], Quan He[1], Hua Gan[2], Tingting Zeng[1], Qiao Liu[1], John F. Moorhead[3], Zac Varghese[3], Nan Ouyang[2] and Xiong Z. Ruan[3,4]

[1]Department of Cardiology, The First Affiliated Hospital of Chongqing Medical University, Chongqing, People's Republic of China; [2]Department of Nephrology, The First Affiliated Hospital of Chongqing Medical University, Chongqing, People's Republic of China; [3]John Moorhead Research Laboratory, Centre for Nephrology, University College London Medical School, Royal Free Campus, London, United Kingdom; and [4]Centre for Lipid Research and Key Laboratory of Molecular Biology for Infectious Diseases (Ministry of Education), Institute for Viral Hepatitis, Department of Infectious Diseases, the Second Affiliated Hospital, Chongqing Medical University, Chongqing, People's Republic of China

Blood phosphate levels are linked to atherosclerotic cardiovascular disease in patients with chronic kidney disease (CKD), but the molecular mechanisms remain unclear. Emerging studies indicate an involvement of hyperphosphatemia in CKD accelerated atherogenesis through disturbed cholesterol homeostasis. Here, we investigated a potential atherogenic role of high phosphate concentrations acting through aberrant activation of sterol regulatory element-binding protein (SREBP) and cleavage-activating protein (SCAP)-SREBP2 signaling in patients with CKD, hyperphosphatemic apolipoprotein E (ApoE) knockout mice, and cultured vascular smooth muscle cells. Hyperphosphatemia correlated positively with increased atherosclerotic cardiovascular disease risk in Chinese patients with CKD and severe atheromatous lesions in the aortas of ApoE knockout mice. Mice arteries had elevated SCAP levels with aberrantly activated SCAP-SREBP2 signaling. Excess phosphate *in vitro* raised the activity of α-mannosidase, resulting in delayed SCAP degradation through promoting complex-type conversion of SCAP N-glycans. The retention of SCAP enhanced transactivation of SREBP2 and expression of 3-hydroxy-3-methyl-glutaryl coenzyme A reductase, boosting intracellular cholesterol synthesis. Elevated α-mannosidase II activity was also observed in the aortas of ApoE knockout mice and the radial arteries of patients with uremia and hyperphosphatemia. High phosphate concentration *in vitro* elevated α-mannosidase II activity in the Golgi, enhanced complex-type conversion of SCAP N-glycans, thereby upregulating intracellular cholesterol synthesis. Thus, our studies explain how hyperphosphatemia independently accelerates atherosclerosis in CKD.

Correspondence: *Nan Ouyang or Xiong Z. Ruan, Department of Nephrology, The First Affiliated Hospital of Chongqing Medical University, Chongqing, People's Republic of China, 400016. E-mail: ouyangnan930@hotmail.com or x.ruan@ucl.ac.uk*

Received 29 March 2020; revised 4 January 2021; accepted 12 January 2021; published online 23 February 2021

Kidney International (2021) **99,** 1342–1353; https://doi.org/10.1016/j.kint.2021.01.016

KEYWORDS: α-mannosidase activity; atherosclerosis; HMGCR; hyperphosphatemia; SCAP N-glycans conversion

Translational Statement

Hyperphosphatemia accelerates atherosclerotic cardiovascular disease, but the underlying mechanisms are still unclear. This paper describes a new mechanism by which hyperphosphatemia increased the activity of α-mannosidase II in the Golgi, which enhanced sterol regulatory element-binding protein (SREBP) cleavage-activating protein (SCAP)–mediated SREBP2 activation in lipid synthesis by modulating SCAP N-glycans. Our work provides a mechanistic explanation for a high incidence of atherosclerotic cardiovascular disease in patients with chronic kidney disease and the underlying mechanisms by which phosphate directly affects vessel lipid homeostasis without changing blood lipid levels. It may also contribute to the design of effective dual therapeutic strategies targeting both phosphate and lipid metabolisms in the chronic kidney disease population.

Atherosclerotic cardiovascular disease (ASCVD) is the leading cause of mortality in patients with chronic kidney disease (CKD).[1] Cholesterol blood levels in patients with CKD are usually normal or even low but are associated with extraordinarily high ASCVD risk.[2] This clinical phenomenon implies that cholesterol metabolism in patients with CKD differs from that of the general population and that nonclassical risk factors may disrupt lipid

homeostasis in CKD to significantly increase ASCVD by unknown mechanisms.[2–5]

Phosphate, whose level is tightly regulated in the human body (physiologic range 0.8–1.5 mmol/l), plays vital roles in the regulation of various physiological processes such as membrane integrity, intracellular signaling, and skeletal mineralization.[6–8] Hyperphosphatemia accounts for morbidity in 23% of patients with stage 4 CKD and about 70% of patients on dialysis.[9] Compelling clinical evidence suggests that hyperphosphatemia contributes to higher atherosclerotic death risk in Western patients with CKD and the general population.[10–12] Moreover, feeding apolipoprotein E (apoE)$^{-/-}$ mice a phosphate-rich diet resulted in more severe atherosclerotic lesions independently of vascular calcification, whereas oral phosphate binder could decrease the progression of atherosclerosis in uremic apoE$^{-/-}$ mice.[13–15] Emerging studies indicate the involvement of hyperphosphatemia in atherogenesis in CKD through disturbed cholesterol homeostasis,[16,17] but the underlying mechanisms remain largely unknown.

Sterol regulatory element-binding protein 2 (SREBP2), which is synthesized as an immature precursor embedded in the endoplasmic reticulum (ER), principally controls the expression of genes involved in cholesterol uptake and biosynthesis. The stability and maturation of precursor SREBP2 relies on binding to SREBP cleavage-activating protein (SCAP), a sterol sensor.[18,19] A small reduction of ER membrane cholesterol alters SCAP conformation, resulting in its detachment from its anchoring protein insulin-induced gene 1 (INSIG1) and translocation of SCAP/SREBP2 complex from ER to Golgi, where SREBP2 is enzymatically cleaved and releases its active NH_2 terminal fragment SREBP2-N. SREBP2-N can enter the nucleus to bind with an SRE to activate 3-hydroxy-3-methyl-glutaryl coenzyme A reductase (HMGCR) and low-density lipoprotein receptor (LDLr) gene transcription.[20,21] Intracellular cholesterol *de novo* synthesis is increased via upregulated HMGCR, and native LDL intake is strengthened by upregulated LDLr.

During translocation to the Golgi, asparagine (N)-linked carbohydrates of SCAP are successively modified by α-mannosidase (α-MAN) I, N-acetylglucosamine (GlcNAc) transferase I, and α-MAN II.[22] The modifications cause the N-glycans of SCAP to be heterogeneously converted from a format of high-mannose glycans to complex glycans containing multiple branches (defined as "complex-type conversion"). Part of the SCAP protein then recycles back to the ER to form a new complex with another SREBP2, while the remainder is subject to degradation by the ubiquitin proteasome system.[23] Glucose deprivation prohibited N-glycosylation of SCAP, which made it more susceptible to degradation and therefore restricted its biofunction in the transactivation of SREBPs.[24] Increased biosynthesis of cholesterol mediated by HMGCR contributes to lipid accumulation and foam cell formation in vascular smooth muscle cells (VSMCs).[25] SCAP dysfunction has been implicated in atherosclerosis observed in chronic inflammatory status and diabetes.[25–29] However, whether increased serum phosphate (P^{3+}) level in patients with CKD affects SCAP posttranslational glycosylation, and whether the modifications contribute to the development of ASCVD remains unclear.

In the present study, we analyzed clinical epidemiology data from a Chinese CKD population, which supported our argument that hyperphosphatemia accelerated ASCVD. We also explored the aberrant activation of SCAP-SREBP2 signaling in the arteries of hyperphosphatemic apoE$^{-/-}$ mice and uremic patients. We sought to determine how excessive phosphate perturbs SCAP posttranslational glycosylation, causing unregulated intracellular cholesterol synthesis with foam cell formation. These studies provide a novel mechanistic explanation for the accelerated atherosclerosis in the CKD population.

METHODS

A cross-sectional study in Chinese CKD population

A study population including 438 patients with CKD from stage 3 to 5 admitted to the First Affiliated Hospital of Chongqing Medical University from January 1, 2013 to February 28, 2016. Serum P^{3+} levels were the mean of 3 measurements of fasting morning serum P^{3+} concentration within 1 month. All the subjects were categorized into 4 serum P^{3+} ranges as follows: <1.21 mmol/l, 1.22 mmol/l to ~1.46 mmol/l, 1.47 mmol/l to ~1.78 mmol/l, and >1.78 mmol/l, by quartile spacing strategy. Details are described in the Supplementary Methods. The study was approved by the Human Research Ethics Committee at Chongqing Medical University. All subjects were included after providing informed consent.

Study animals

A hyperphosphatemic animal model was established by feeding high-phosphate diet (HPD) as previously published.[13] Eight-week-old male apoE$^{-/-}$ mice were raised with standard chow (n = 15) or HPD (n = 15) (Baitai Hongda Biotec, Jiangsu, China) for 16 weeks. The formulas of the main nutrition gradients were shown in Supplementary Table S1. The post valve aortic root (about 5 mm in length) was used to prepare frozen serial sections. The remaining aortas were stored in −80 °C for mRNA and protein examination. All procedures of the animal study were approved by the Subcommittee on Animal Care Research at Chongqing Medical University.

Cell culture

The detailed methods of our primary human aortic VSMCs culture were based on our previous work.[25] The cells of sixth or seventh passages were used for experiments. Phosphate stocking medium was made of NaH_2PO_4 and Na_2HPO_4 (adjusting pH to 7.40).

SCAP protein degradation

The protocols for determining SCAP protein degradation followed previous investigations.[24,26]

Crude ER isolation and examination of SCAP N-glycans

Treated VSMCs on 4 150-cm^2 flasks were harvested to examine the format of SCAP N-glycans following the approach of Nohturfft *et al.*[22]

Table 1 | Multivariate logistic regression analysis of the correlation between serum P^{3+} level and ASCVD risk, stratified by serum P^{3+} levels

Item	β value	*P* value	Odds ratio	95% confidence interval
Serum P^{3+} levels (mmol/l)		0.001		
1.22∼1.46	0.071	0.825	1.073	0.574∼2.007
1.47∼1.78	0.854	0.010	2.348	1.230∼4.481
>1.78	1.057	0.002	2.878	1.479∼5.600

ASCVD, atherosclerotic cardiovascular disease.
Multiple logistic regression models determined with a stepwise procedure, considering all potential predictors and several interactions. Only variables with a significant effect or showing a potentially confounding influence in the model were maintained. *P* values are for significance between groups.

Microsomes preparation and enzymatic assay of α-MAN II activity

Treated VSMCs on 2 150-cm^2 flasks were harvested, and the α-MAN II activity was determined using a previously described enzyme-based method and normalized by microsome proteins determined by the Lowry assay.[26]

Statistics

Statistical analyses were performed using SPSS 13.0 (SPSS, Inc., Chicago, IL). All data were analyzed by 2-tailed Student *t* test as well as by 1-way analysis of variance as appropriate. $P < 0.05$ was considered statistically significant.

RESULTS

Hyperphosphatemia correlated with increased ASCVD risk in Chinese patients with CKD

In this study, 438 patients with CKD were divided into atherosclerosis and nonatherosclerosis groups according to the diagnosis of ASCVD; their basic characteristics are described in Supplementary Table S2. Hyperphosphatemia and several other parameters such as maintenance dialysis showed positive correlations with the incidence of ASCVD (Supplementary Table S3). Multivariate logistic stepwise regression analysis suggested that serum P^{3+} levels between 1.47 mmol/l to ∼1.78 mmol/l ($P = 0.010$) and >1.78 mmol/l ($P = 0.002$) were positively correlated with the incidence of ASCVD. ASCVD risk increased with rising serum P^{3+} level (serum P^{3+} level, 1.47 to ∼1.78 mmol/l; odds ratio, 2.348; serum P^{3+} level, >1.78 mmol/l, odds ratio, 2.878) (Table 1).

Hyperphosphatemia disrupted SCAP mediated cholesterol homeostasis in the atherogenesis of apoE$^{-/-}$ mice

Four weeks after feeding an HPD, the serum P^{3+} levels of the mice were significantly elevated and sustained until sacrificed (HPD 2.68 mmol/l vs. standard chow 2.14 mmol/l). There were no alterations of other indexes such as total cholesterol (TC) and triglyceride when sacrificed, except for parathyroid hormone, the secondary change of elevated serum P^{3+} levels (Supplementary Table S4). HPD feeding resulted in a more severe atheroma burden relative to standard chow (Figure 1a and b). The serum P^{3+} level correlated positively with the atheroma burden in the aortic root (Figure 1c).

We observed transcription changes of cholesterol metabolism-related genes in aortas but not in livers in HPD-fed mice (liver data not shown; primers are shown in Supplementary Table S5). mRNA levels of HMGCR, LDLr, and SREBP2, but not of INSIG1, SCAP, liver X receptor α (LXRα) or adenosine triphosphate–binding cassette transporter A1 (ABCA1), were increased in HPD-fed mice (Figure 1d). The protein levels of SCAP, HMGCR, and SREBP2-N, but not INSIG1, LDLr, LXRα, and ABCA1 were dramatically elevated in HPD-fed mice relative to the control (Figure 1e and f). Moreover, immunohistochemistry staining further confirmed SCAP protein increment in the aortas of HPD-fed mice (Figure 1g).

Excess phosphate induced translocation of SCAP and cholesterol accumulation *in vitro*

VSMCs and macrophages are the main sources of atheromatous foam cells. Neutral lipid deposition was increased when VSMCs and THP-1 macrophages were treated with excess phosphate (3.0 mmol/l) (Figure 2a and Supplementary Figure S1A). The TC and cholesterol ester (CE) levels, but not free cholesterol in excess phosphate-treated VSMCs were significantly higher than in control cells (Figure 2b). Excess phosphate increased intracellular TC but not CE or free cholesterol in THP-1 macrophages (Supplementary Figure S1B).

Excess phosphate increased the mRNA levels of HMGCR, LDLr, and SREBP2, but did not increase levels of INSIG1, LXRα, or ABCA1 (Figure 2c and Supplementary Figure S1C; primers are shown in Supplementary Table S6). It did not affect the protein levels of INSIG1, LDLr, LXRα, and ABCA1, but it did increase that of HMGCR and SREBP2-N (Figure 2d and e and Supplementary Figure S1D and E). Excess phosphate did not affect SCAP mRNA expression (Figure 2h and Supplementary Figure S1H) but increased its protein level (Figure 2f and g and Supplementary Figure S1F and G). Excess phosphate enhanced colocalization of SCAP within the Golgi (Figure 2i and Supplementary Figure S1I). VSMCs were more sensitive to excess phosphate than THP-1 macrophages were, so VSMCs were used alone in subsequent experiments. Levels of LDLr mRNA increased 1.35-fold in excess phosphate-treated VSMCs, but its protein expression reached only 1.16-fold of control. This small variation in LDLr protein level did not increase Dil-LDL uptake as shown by fluorescence photography (Figure 2j) and fluorospectrophotometry (Figure 2k). In line with our *in vivo* findings, we found that excess phosphate increased SCAP protein at the posttranscriptional stage, enhancing SCAP escort for SREBP2 transactivation to upregulate the expression of HMGCR, thus facilitating cholesterol *de novo* synthesis and intracellular cholesterol accumulation.

Excess phosphate promoted intracellular cholesterol accumulation via SCAP-SREBP2-HMGCR pathway in VSMCs

The mRNA levels of HMGCR and SREBP2 were stably increased when the concentration of phosphate rose from 1.0

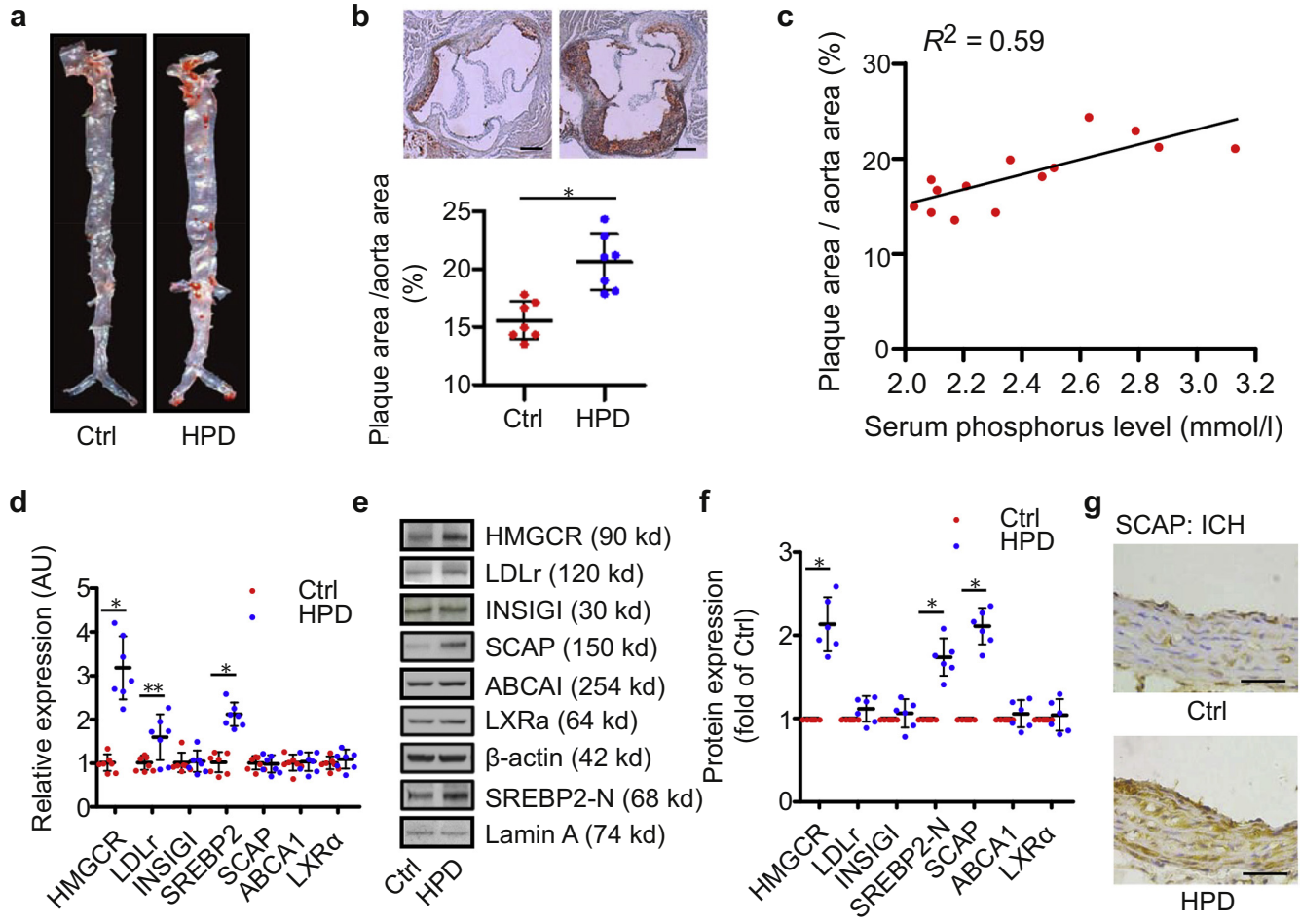

Figure 1 | Hyperphosphatemia promoted atherosclerosis and disrupted sterol regulatory element-binding protein (SREBP) cleavage-activating protein (SCAP)–mediated cholesterol homeostasis in the aorta of apolipoprotein E (apoE)$^{-/-}$ mice. (**a,b**) The hyperphosphatemia model was established by feeding apoE$^{-/-}$ mice with high-phosphate diet (HPD), whose littermates receiving normal chow served as a control (Ctrl). The longitudinal dissection of the aortic tissue– or aortic root–frozen serial sections of the mice were prepared and stained by Oil Red O method when they were killed. (**a**) Representative images of atheroma lesions on the longitudinal dissection of the aorta, photographed by a camera (Canon, Tokyo, Japan) ($n = 6$ mice per group). (**b**) Representative images of atheroma lesions on the aortic root sections of mice, observed under microscopy; quantification of the atheroma burden was processed on 6 sections of each aorta by ImageJ software (National Institutes of Health, Bethesda, MD); each section was from every 10 successive sections of 1 mouse. The results were means ± SD of plaque area/aorta area (%) ($n = 7$ mice per group). Bars = 100 μm. (**c**) The correlation between atheroma burden and serum phosphate level, analyzed by linear regression analysis ($n = 14$ mice). (**d**) The mRNA expression of the cholesterol metabolic components analyzed by real-time polymerase chain reaction; β-actin served as the reference gene. Values are means ± SD from 7 mice of each group. (**e**) The protein levels of the cholesterol metabolic components examined by Western blotting; the demonstrated bands were typical from 3 experimental repeats. β-Actin served as the domestic control for the cytoplasmic protein, and lamin A served as the reference for the nuclear protein. (**f**) The densitometric scans of protein bands are represented by means ± SD, normalized by comparison with reference protein and expressed as a percentage of control ($n = 6$ mice per group). (**g**) Representative photomicrographs of SCAP antibody-stained immunohistochemistry (ICH) sections from the mice aortic root ($n = 6$ mice per group). Bars = 100 μm. Statistical significance was assessed using a 2-tailed Student t test (**b,d,f**). *$P < 0.01$; **$P < 0.05$. ABCA1, adenosine triphosphate–binding cassette transporter A1; AU, arbitrary unit; HMGCR, 3-hydroxy-3-methyl-glutaryl coenzyme A reductase; INSIG1, insulin-induced gene 1; LDLr, low-density lipoprotein receptor; LXRα, liver X receptor α; SREBP2-N, NH_2 terminal fragment of SREBP2. To optimize viewing of this image, please see the online version of this article at www.kidney-international.org.

to 5.0 mmol/l without affecting SCAP mRNA levels (Supplementary Figure S2A). HMGCR and SCAP protein increased as the phosphate concentration elevated (Supplementary Figure S2B), suggesting a dose-dependent SCAP response to phosphate signaling. A physiological phosphate concentration (1.0 mmol/l) changed neither SCAP nor HMGCR protein levels over the 72-hour time course, but excess phosphate increased HMGCR and SCAP protein levels dramatically and they remained high after 24 hours (Supplementary Figure S2C).

Sodium-dependent phosphate cotransporter is the main channel for phosphate uptake in VSMCs, to which phosphoformate sodium (PFA) is a specific competitive inhibitor that can dose-dependently block sodium-dependent phosphate

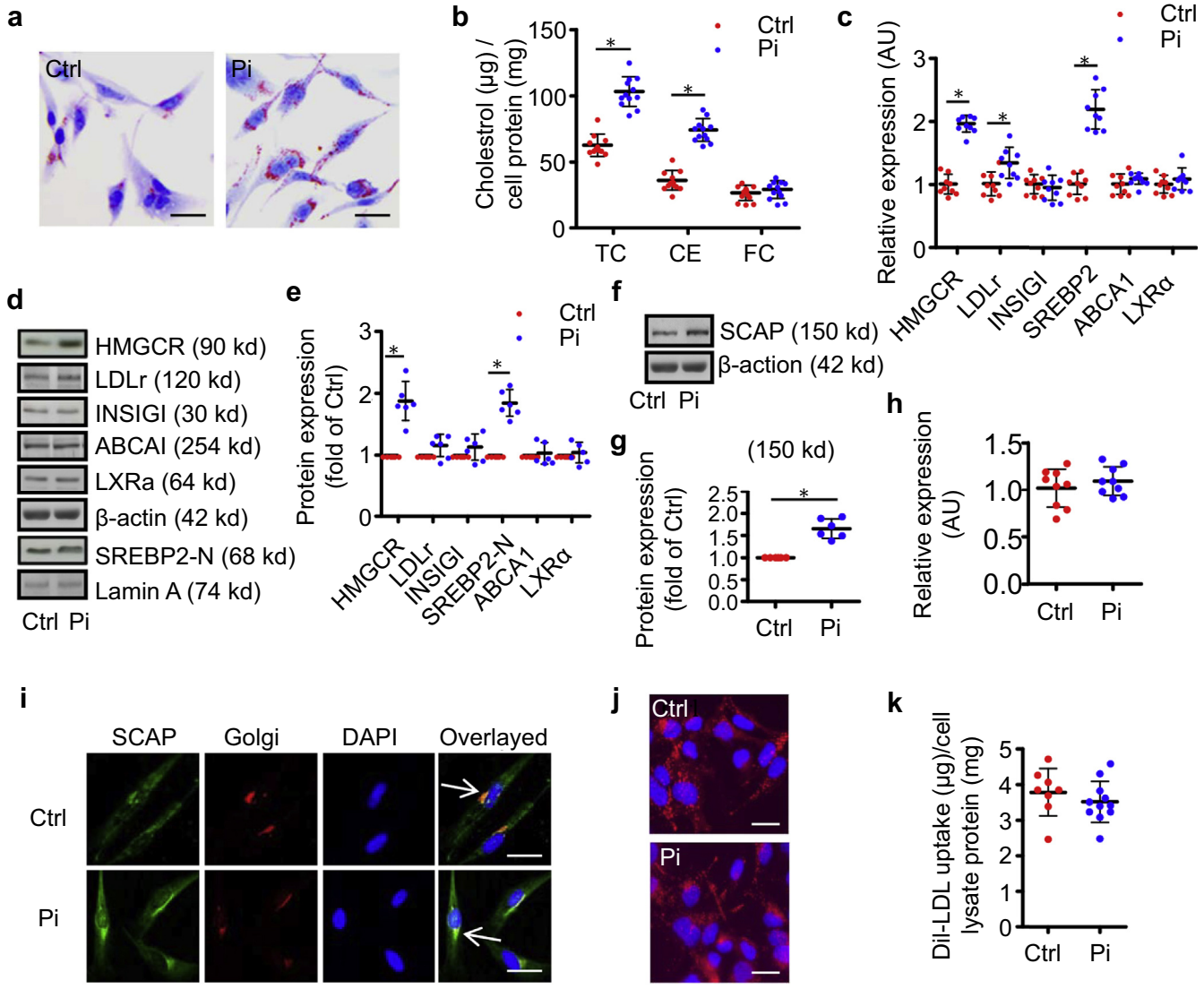

Figure 2 | Excess phosphate (Pi) induced translocation of sterol regulatory element-binding protein (SREBP) cleavage-activating protein (SCAP) and cholesterol accumulation in vascular smooth muscle cells (VSMCs). (**a–i**). The VSMCs were cultured in experimental medium with or without Pi for 24 hours. (**a**) The intracellular neutral lipids were stained by Oil Red O. The results are typical of those observed in 4 separate experiments. Bars = 50 μm. (**b**) Quantification of intracellular free cholesterol (FC) and cholesterol ester (CE). Values are means ± SD from 3 experimental repeats ($n = 12$ per group). (**c,h**) The gene expressions of the cholesterol metabolic components determined by real-time polymerase chain reaction. β-Actin served as the reference gene. Values are means ± SD from 3 experimental repeats ($n = 9$ per group). (**d,f**) The protein levels of the cholesterol metabolic components examined by Western blotting. The demonstrated bands were typical from 3 experimental repeats. β-Actin served as the domestic control for the cytoplasmic protein, and lamin A served as the reference for the nuclear protein. (**e,g**) The densitometric scans of protein bands represented by means ± SD from 3 experimental repeats ($n = 6$ per group), normalized by comparison with reference protein and expressed as a percentage of control (Ctrl). (**i**) The colocalization of SCAP with Golgi apparatus observed by confocal microscopy (arrows). The results are typical of those observed in 4 separate experiments. Bars = 50 μm. (**j,k**). The VSMCs were incubated with Dil–low-density lipoprotein (LDL) (25 μmol/l) for 4 hours. (**j**) Cells were fixed with 4% paraformaldehyde and captured by fluorescence microscopy; the red fluorescence represents Dil-LDL uptake via low-density lipoprotein receptor (LDLr). Bars = 100 μm. (**k**) Cell protein were prepared with lysis buffer; Dil-LDL fluorescence intensity were quantified by fluorescence spectrophotometer. The histogram represents means ± SD of Dil-LDL fluorescence intensity from 3 experimental repeats ($n = 12$ per group), normalized by total protein volume. Statistical significance was assessed using a 2-tailed Student t test (**b,c,e,g,h,k**). $^*P < 0.01$; $^{**}P < 0.05$. ABCA1, adenosine triphosphate–binding cassette transporter A1; AU, arbitrary unit; DAPI, 4′,6-diamidino-2-phenylindole; HMGCR, 3-hydroxy-3-methyl-glutaryl coenzyme A reductase; ICH, immunohistochemistry; INSIG1, insulin-induced gene 1; LXRα, liver X receptor α; SREBP2-N, NH_2 terminal fragment of SREBP2; TC, total cholesterol. To optimize viewing of this image, please see the online version of this article at www.kidney-international.org.

cotransporter.[30] PFA did not reduce HMGCR and SREBP2 mRNA levels with a physiological concentration of phosphate, but PFA inhibited their excess phosphate elevated expressions (Figure 3a and b). PFA did not affect SCAP mRNA levels (Figure 3a), but it overrode the increased SCAP, HMGCR, and SREBP2-N protein levels observed after excess phosphate

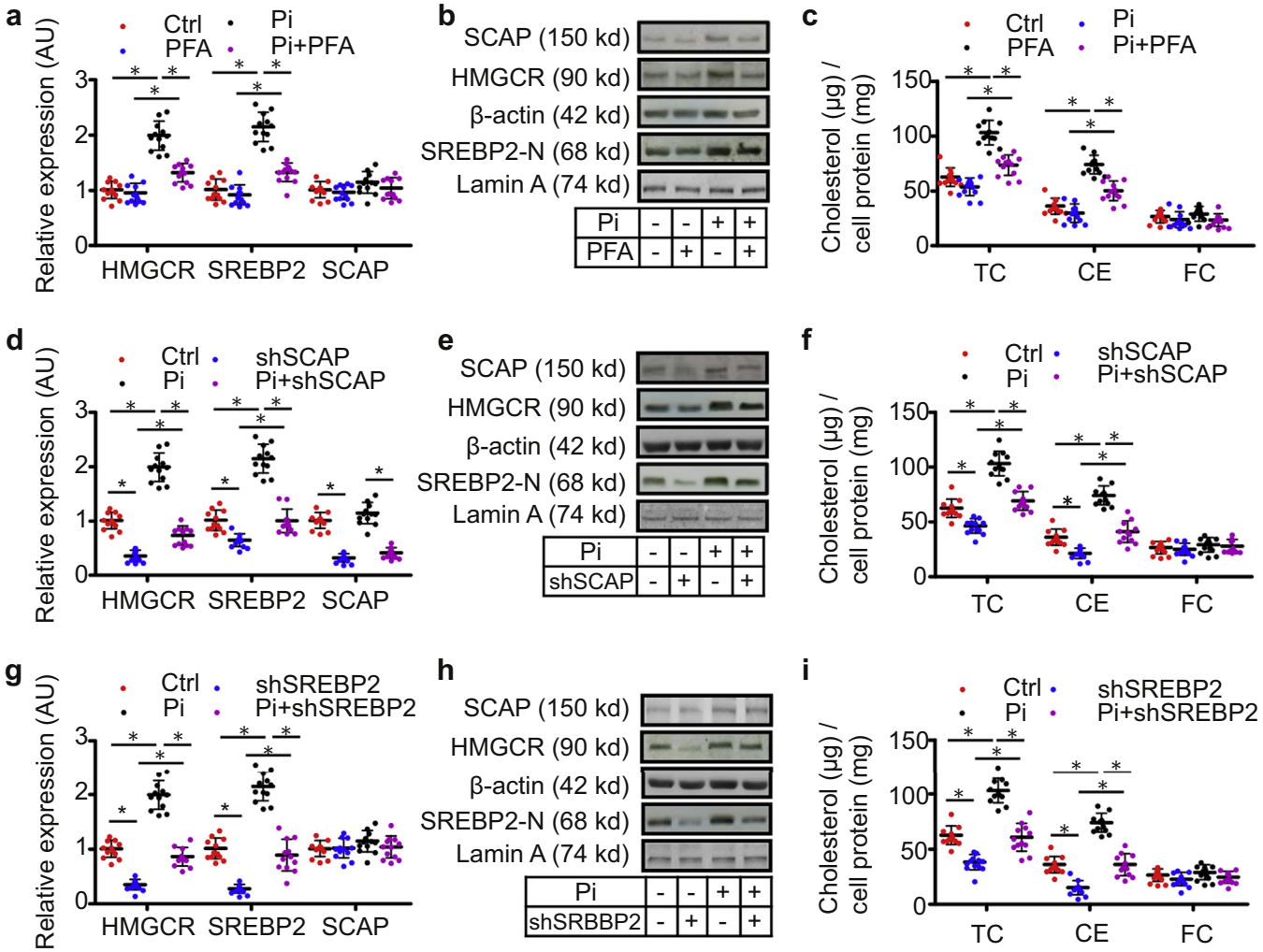

Figure 3 | Excess phosphate (Pi) promoted intracellular cholesterol accumulation via sterol regulatory element-binding protein (SREBP) cleavage-activating protein (SCAP)–SREBP2–3-hydroxy-3-methyl-glutaryl coenzyme A reductase (HMGCR) pathway in vascular smooth muscle cells (VSMCs). The VSMCs were cultured in experimental medium with or without Pi and indicated treatments for 24 hours. (**a,d,g**) The gene expression determined by real-time polymerase chain reaction. β-Actin served as the reference gene. Values are means ± SD from 3 experimental repeats ($n = 12$). (**b,e,h**) The protein levels examined by Western blotting. The demonstrated bands were typical from 3 experimental repeats. β-Actin served as the reference for cytoplasmic proteins, and lamin A served as the reference for proteins in the nucleus. (**c,f,i**) Quantification of intracellular free cholesterol (FC) and cholesterol ester (CE). Values are means ± SD of duplicate wells from 3 experimental repeats ($n = 12$). Statistical significance was assessed using 1-way analysis of variance with Bonferroni or Tamhane T_2 as appropriate (**a,d,f,g,i,j,l**). *$P < 0.01$. AU, arbitrary unit; Ctrl, control; PFA, phosphoformate sodium; sh, short hairpin; SREBP2-N, NH_2 terminal fragment of SREBP2; TC, total cholesterol.

treatment (Figure 3b). Meanwhile, PFA inhibited intracellular TC and CE accumulation induced by excess phosphate, but it did not change their levels within the physiological concentration of phosphate (Figure 3c). These results imply that blocking VSMC phosphate uptake can abrogate the activation of SCAP signaling by excess phosphate.

When knocking down SCAP by short hairpin RNA (shRNA), the mRNA and protein levels of HMGCR and SCAP decreased, even in the presence of excess phosphate, which also reduced SREBP2 mRNA level and SREBP2-N in the nucleus (Figure 3d and e). Meanwhile, knocking down SCAP reduced intracellular TC and CE contents (Figure 3f). Knocking down SREBP2 led to much-reduced mRNA levels of HMGCR and SREBP2 but not of SCAP, even in the presence of excess phosphate (Figure 3g). Excess phosphate increased SCAP protein level but knocking down SREBP2 decreased HMGCR and SREBP2-N in the nucleus (Figure 3h). Moreover, knocking down SREBP2 reduced intracellular TC and CE content and offset the accumulating effects on them of excess phosphate (Figure 3i). These results indicated that excess phosphate specifically promoted cholesterol accumulation in VSMCs via SCAP-SREBP2-HMGCR signaling.

Excess phosphate delayed SCAP degradation by promoting complex-type conversion of its N-glycans

Cycloheximide is an inhibitor for intracellular protein synthesis, which can be used to determine the half-life of

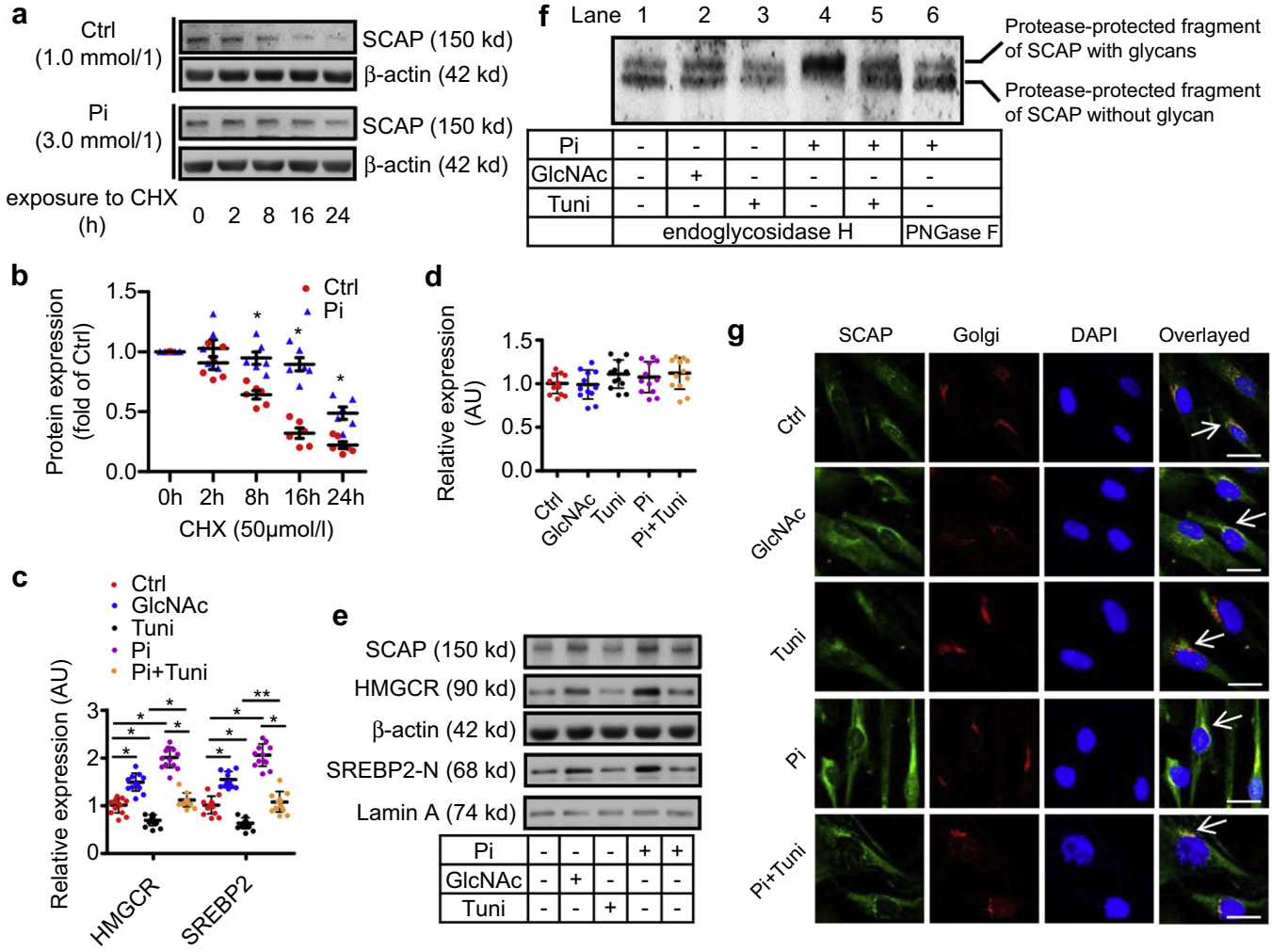

Figure 4 | Excess phosphate (Pi) delayed sterol regulatory element-binding protein (SREBP) cleavage-activating protein (SCAP) degradation by promoting complex-type conversion of its N-glycans. (**a,b**) The vascular smooth muscle cells (VSMCs) were cultured in experimental medium with 50 μmol/l cycloheximide (CHX) in the absence or presence of Pi for the indicated times. (**a**) The protein levels were examined by Western blotting. The demonstrated bands were typical from 3 experimental repeats. (**b**) The densitometric scans of protein bands were processed by ImageJ software (National Institutes of Health, Bethesda, MD). Values are means ± SD from 3 experiments ($n = 6$). (**c–g**) The VSMCs were cultured in experimental medium with or without Pi and indicated treatments for 24 hours. (**c,d**) The gene expression was determined by real-time polymerase chain reaction. β-Actin served as the reference gene. Values are means ± SD from 3 experiments ($n = 12$). (**e**) The protein levels examined by Western blotting. The demonstrated bands were typical from 3 experimental repeats. Lamin A served as the reference for proteins in the nucleus. β-Actin served as the reference for cytoplasmic proteins. (**f**) N-glycans of SCAP were analyzed as described in the Methods section. (**g**) The colocalization of SCAP with Golgi apparatus was observed by confocal microscopy (arrows). The results are typical of those observed in 4 separate experiments. Bars = 50 μm. Statistical significance was assessed using 1-way analysis of variance with Bonferroni or Tamhane T_2 as appropriate (**b–d**). *$P < 0.01$; **$P < 0.05$. AU, arbitrary unit; Ctrl, control; DAPI, 4′,6-diamidino-2-phenylindole; GlcNAc, N-acetylglucosamine; HMGCR, 3-hydroxy-3-methyl-glutaryl coenzyme A reductase; PNGase, peptide:N-glycosidase; SREBP2-N, NH_2 terminal fragment of SREBP2; Tuni, tunicamycin. To optimize viewing of this image, please see the online version of this article at www.kidney-international.org.

proteins in molecular biology.[24,26] SCAP protein levels significantly decreased at the 8th hour after cycloheximide treatment and reduced to 22% at the 24th hour compared to that of hour 0 within a physiological phosphate concentration. However, with excess phosphate, the SCAP protein at the 24th hour remained at 48.9% of that at hour 0 (Figure 4a and b), indicating that excess phosphate increased SCAP protein retention by delaying its degradation. GlcNAc (20 mmol/l), which facilitates N-glycosylation, significantly increased mRNA levels of HMGCR and SREBP2, while tunicamycin (Tuni; 1 μg/ml, an inhibitor of N-glycosylation) decreased them even in the presence of excess phosphate (Figure 4c). Neither GlcNAc nor Tuni altered the mRNA level of SCAP (Figure 4d). However, GlcNAc increased SCAP, HMGCR, and SREBP2-N protein levels equivalent to those of excess phosphate, and Tuni decreased them in the same condition (Figure 4e). These data implied that the effects of excess phosphate on SCAP signaling were probably mediated by altering the N-glycans of SCAP.

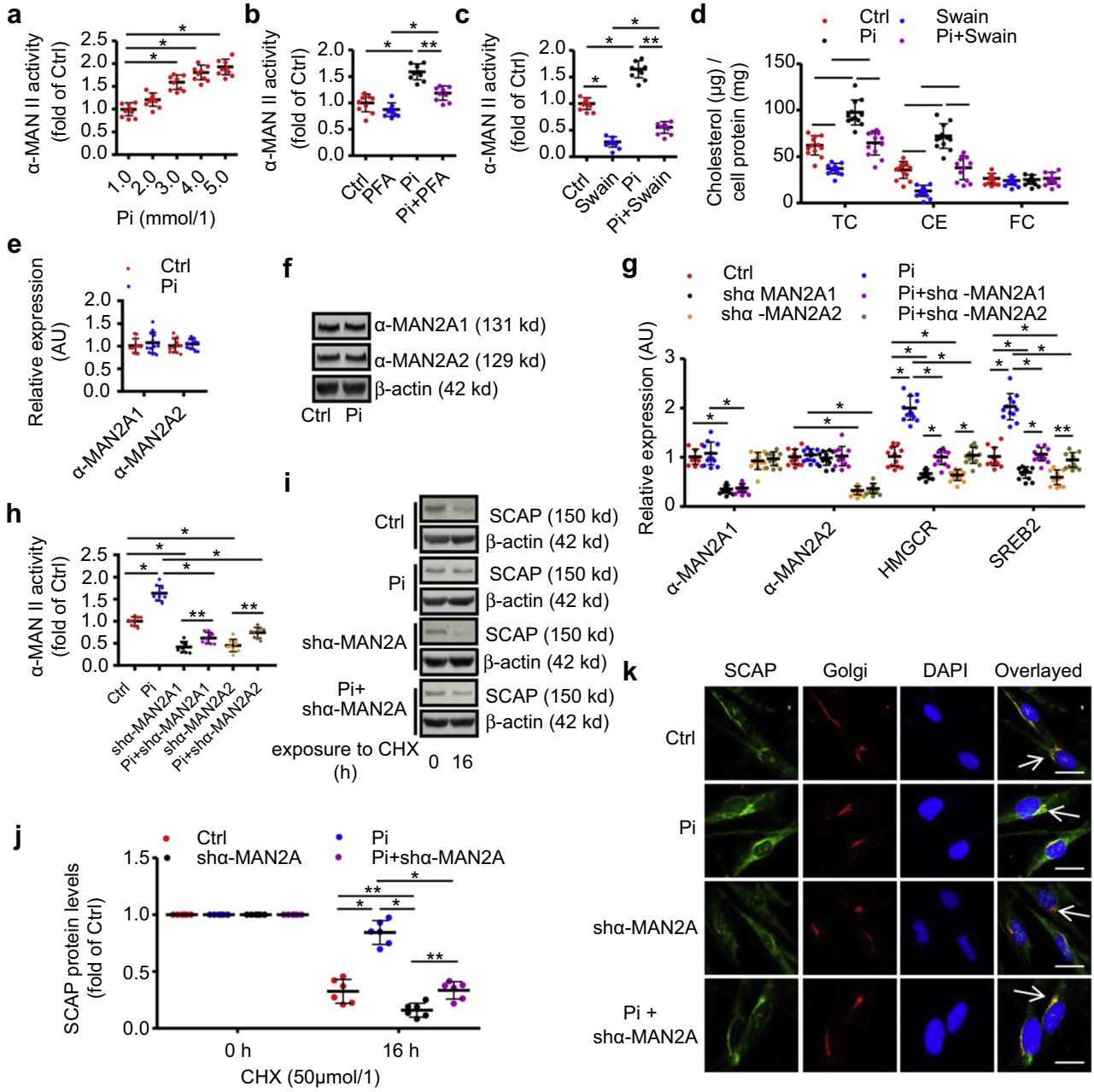

Figure 5 | Excess phosphate (Pi) enhanced the activity of α-mannosidase II isoform A1 (α-MAN 2A1) and α-MAN 2A2 *in vitro*. (**a–h,k**) The vascular smooth muscle cells (VSMCs) were cultured in experimental medium with or without Pi and indicated treatments for 24 hours. (**a,b,c,h**) The activity of α-MAN II determined by the enzymatic assay as described in the Methods section. Values are means ± SD of duplicate wells from 3 experiments ($n = 9$). (**d**) Intracellular free cholesterol (FC) and cholesterol ester (CE) assayed by a quantitative method. Values are means ± SD of duplicate wells from 3 experiments ($n = 12$). (**e,g**) The gene expression was determined by real-time polymerase chain reaction. β-Actin served as the reference gene. Values are means ± SD of duplicate wells from 3 experiments ($n = 12$). (**f**) The protein levels were examined by Western blotting. The demonstrated bands were typical from 3 experimental repeats. β-Actin served as the reference for cytoplasmic proteins. (**k**) The colocalization of sterol regulatory element-binding protein (SREBP) cleavage-activating protein (SCAP) with Golgi apparatus observed by confocal microscopy (arrows). The results are typical of those observed in 4 separate experiments. Bars = 50 μm. (**i,j**) The VSMCs were cultured in experimental medium with 50 μmol/l cycloheximide (CHX) in the absence or presence of Pi and transfection of both short hairpin RNA (shRNA) for α-MAN 2A1 and 2A2 for 16 hours. (**i**) The SCAP protein levels were examined by Western blotting. The demonstrated bands were typical from 3 experimental repeats. (**j**) The densitometric scans of SCAP protein bands were processed by ImageJ software (National Institutes of Health, Bethesda, MD). Values are means ± SD of duplicate wells from 3 experiments ($n = 6$). Statistical significance was assessed using 1-way analysis of variance with Bonferroni or Tamhane T_2 as appropriate (**a–d,g,j**) and a 2-tailed Student *t* test (**e**). $^*P < 0.01$; $^{**}P < 0.05$. AU, arbitrary unit; Ctrl, control; DAPI, 4′,6-diamidino-2-phenylindole; HMGCR, 3-hydroxy-3-methyl-glutaryl coenzyme A reductase; PFA, phosphoformate sodium; Swain, swainsonine; TC, total cholesterol. To optimize viewing of this image, please see the online version of this article at www.kidney-international.org.

SCAP contains a glycosylated peptide of 170 amino acids that is protected from proteolysis by trypsin.[31] This trypsin-protected fragment acquires 2 N-linked high-mannose-type glycans that are sensitive to hydrolysis by endoglycosidase H (endo H) when the nascent SCAP was synthesized. The 2 glycans will become endo H–resistant when further modified by a-MAN II in the Golgi, converting to the complex-type glycans.[22] Within the physiological phosphate concentration, N-glycans of SCAP largely remained high-mannose-type, as shown that the apparent mass of the most trypsin-protected fragments became smaller (without glycans) after endo-H digestion, which hydrolyzed their high-mannose-type glycans (Figure 4f, lane 1). Excess phosphate converted >90% of SCAP N-glycans to the complex type, because most trypsin-protected fragments are still with glycans after endo H digestion (endo H resistant) (Figure 4f, lane 4 vs. lane 1). Excess phosphate was more efficient than GlcNAc in facilitating the complex-type conversion of SCAP N-glycans (Figure 4f, lane 4 vs. lane 2). Tuni nearly abolished phosphate-induced conversion of SCAP N-glycans from high-mannose-type to the complex-type, as shown by half of the trypsin-protected fragments remaining sensitive to endo H (Figure 4f, lane 5 vs. lane 4), which hydrolyzed them to make the apparent mass of the fragments as small as if N-glycans had been removed, whether or not they have been modified in the Golgi, using endoglycosidase peptide:N-glycosidase F (as a positive control) (Figure 4f, lane 6). Interestingly, we found that both GlcNAc and excess phosphate increased SCAP colocalization with Golgi apparatus (Figure 4g, GlcNAc and excess phosphate vs. control), which was attenuated by Tuni (Figure 4g, Tuni vs. control), even in the presence of excess phosphate (Figure 4g, Tuni vs. excess phosphate + Tuni).

Excess phosphate enhanced the activity of α-MAN 2A1 and 2A2 *in vitro*

With the increase of phosphate concentrations, α-MAN II activity increased (Figure 5a). Interestingly, PFA did not affect α-MAN II activity within physiological phosphate concentrations, but PFA could reverse the elevated enzyme activity by excess phosphate (Figure 5b). Swainsonine is a potent and selective inhibitor of α-MAN II. Excess phosphate significantly increased the activity of α-MAN II, which can be inhibited by swainsonine (2.5 μg/ml) (Figure 5c). This inhibition also reduced TC and CE levels, even in the presence of excess phosphate (Figure 5d).

α-MAN 2A1 and 2A2 are the 2 isoforms of α-MAN II, which are located mainly in the Golgi and manipulate complex-type conversion of SCAP N-glycans.[32,33] Excess phosphate did not affect either the gene (Figure 5e) or protein (Figure 5f) levels of α-MAN 2A1 and α-MAN 2A2. However, knocking down either α-MAN 2A1 or α-MAN 2A2 with shRNA suppressed both HMGCR and SREBP2 mRNA expression, which can be reversed by excess phosphate (Figure 5g). In the same manner, knocking down either α-MAN 2A1 or α-MAN 2A2 with an shRNA significantly decreased α-MAN II activity, and the effects can be alleviated by excess phosphate (Figure 5h). Knocking down the 2 isoforms simultaneously with both shRNA resulted in accelerated SCAP degradation after cycloheximide treatment, and this effect can be disrupted by excess phosphate (Figure 5i and j). Knocking down the 2 isoforms simultaneously also reduced SCAP colocalization with Golgi, which was reversed by excess phosphate (Figure 5k).

Hyperphosphatemia enhanced the activity of arterial α-MAN II

Hyperphosphatemia did not affect the levels of the genes (Figure 6a) and proteins (Figure 6b) of α-MAN 2A1 and α-MAN 2A2, but it significantly increased α-MAN II activity in the aorta of apoE$^{-/-}$ mice (Figure 6c). We also detected elevated SCAP protein levels in radial arteries of uremic patients with hyperphosphatemia (with serum phosphate level of 2.43 ± 0.57 mmol/l) by immunohistochemistry staining (Figure 6d). There was increased activity of α-MAN II, when compared with the control group (with serum phosphate level of 1.27 ± 0.15 mmol/l) (Figure 6e).

DISCUSSION

In this study, we report for the first time that hyperphosphatemia in Chinese patients with CKD is an independent risk factor for ASCVD and that higher serum P^{3+} levels are significantly associated with a higher ASCVD risk, which accords with clinical observations in Western countries.[10–12] Our present work using a mouse model also revealed evidence that the severity of the aortic atheroma burden paralleled serum P^{3+} levels. These results demonstrated a clear link between hyperphosphatemia and ASCVD.

The known mechanisms involved in the pathophysiology of phosphate-induced cardiovascular risk are vascular calcification and endothelial dysfunction,[7,8,34] but the potential link between hyperphosphatemia and atherosclerosis is reportedly uncertain.[14] Previous studies by Phan *et al.*[14] and Ellam *et al.*[13] both showed that hyperphosphatemia accelerates atherogenesis in apoE$^{-/-}$ mice, but the molecular mechanisms remain unclear. Our data obtained in the present study confirmed the proatherosclerotic effect of hyperphosphatemia and showed for the first time that phosphate has a direct proatherogenic role by perturbing VSMC local cholesterol metabolism. We did not detect significant changes in blood lipid levels in our hyperphosphatemic mouse model, but aortic atheroma lesions increased significantly. In line with this observation, the lipid profile was not affected by a HPD in the study from Ellam *et al.*,[13] and sevelamer benefited atherogenesis in uremic apoE$^{-/-}$ mice with hyperphosphatemia without impacting circulating cholesterol as in the study from Phan *et al.*[14] and Nikolov *et al.*[15] These studies suggest that atherosclerosis induced by hyperphosphatemia is not necessarily dependent on hyperlipidemia and that disturbed cholesterol homeostasis (e.g., increased intracellular cholesterol synthesis) of local cells on the vessel wall could lead to an accumulation of cholesterol in the arteries. In fact, local vascular lipid homeostasis could be

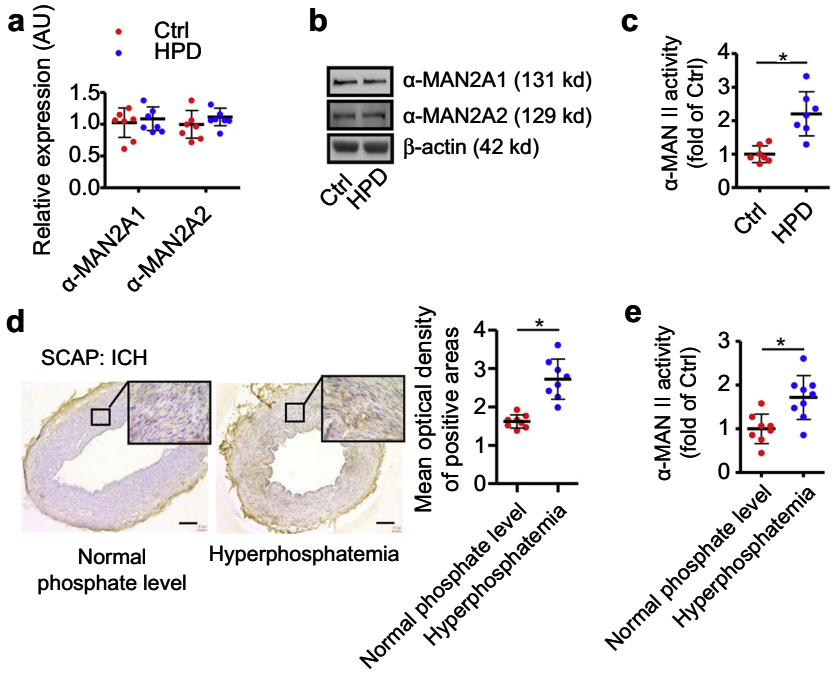

Figure 6 | Hyperphosphatemia enhanced the activity of α-mannosidase (α-MAN) II in the artery. (**a**) The mRNA was extracted from the aorta tissue of the hyperphosphatemia mice and control (Ctrl). The gene expression was analyzed by real-time polymerase chain reaction method. β-Actin served as the reference gene. Values are means ± SD from 7 mice of each group. (**b**) The protein was extracted from the aorta, and the protein levels were examined by Western blotting. The demonstrated bands were typical from 3 experimental repeats ($n = 6$ mice). β-Actin served as the loading control. (**c**) The activity of α-MAN II in the aorta tissue of apolipoprotein $E^{-/-}$ mice. Values are means ± SD from 7 mice of each group. (**d**) Representative photomicrographs of sterol regulatory element-binding protein cleavage-activating protein (SCAP) antibody-stained immunohistochemistry (ICH) sections from the radial artery of uremic patients. Bars = 100 μm. The values of semiquantitative analysis for the positive areas are expressed as the means ± SD from 8 patients at each group. (**e**) The activity of α-MAN II in the radial artery of uremia patients. Values are means ± SD from 8 to 9 patients of each group. Statistical significance was assessed using a 2-tailed Student *t* test (**a,c,e**). *$P < 0.01$. α-MAN 2A1, α-mannosidase II isoform A1; AU, arbitrary unit; HPD, high-phosphate diet. To optimize viewing of this image, please see the online version of this article at www.kidney-international.org.

affected by phosphate or other factors (e.g., inflammation) without changes of overall lipid profiles.[25,28] We and others have demonstrated a weak association between LDL cholesterol level and coronary risk in CKD.[2,35]

Modified LDL uptake via CD36 and scavenger receptor A was thought to be the main pathway for atherogenic cholesterol accumulation in artery cells.[36] However, intracellular cholesterol homeostasis is coordinately regulated by cholesterol influx, cholesterol efflux, and *de novo* cholesterol synthesis. Emerging evidence has highlighted the importance of HMGCR-mediated cholesterol biosynthesis in atherogenesis.[25,37,38] Excess phosphate significantly increased both mRNA and protein expression of HMGCR in VSMCs and macrophages. The elevation of HMGCR level was proven to directly lead to its increased activity for catalyzing acetyl-CoA into mevalonic acid, the rate-limiting step in cholesterol *de novo* synthesis and exacerbating cholesterol accumulation.[24] Meanwhile, excess phosphate neither increased LDL uptake via LDLr nor affected LXRα and ABCA1 expression, which mediates cholesterol efflux from cells. Therefore, the cholesterol accumulation observed in this study was mainly because of increased *de novo* cholesterol synthesis by HMGCR.

By generating the heterozygote SM22α-Cre:$SCAP^{flox/+}$:$apoE^{-/-}$ mice, we have previously reported the importance of SCAP in atherosclerotic foam cell formation in *vivo*.[27] Here, blocking phosphate transport by PFA and gene silencing of SCAP or SREBP2 dramatically interrupted the effect of excess phosphate on SCAP/SREBP2 signaling and cholesterol accumulation, indicating that SCAP may act as a key phosphate-responsive protein, which orchestrates cholesterol homeostasis by controlling SREBP2 activation.

The biosynthesis of N-glycans begins when nascent SCAP is translocated into the lumen of the ER.[22,39] Before SCAP transits to the Golgi, its glycan structure is cleaved by α-MAN I in the ER.[22,39] These high-mannose-type glycans are sensitive to endo H digestion.[40] The glycans can then be catalyzed by GlcNAc transferase I in the medial Golgi, which allows for the generation of glycan branches. Successively, the glycans are converted to multibranched, complex-type glycans by decorations of sialic acid, galactose, and fucose in the trans-Golgi, which is catalyzed by α-MAN II (2A1 and 2A2). They then became resistant to endo H,[22,41] suggesting that α-MAN II is the key enzyme for the formation of SCAP complex-type glycans.

Excess phosphate raised the activity of α-MAN II, leading to the conversion of most SCAP glycans from the high-mannose-type to the complex-type (Figure 4f, lane 4). Gene silencing of α-MAN 2A1 and α-MAN 2A2 blocked this conversion, which further differentiated the detrimental role

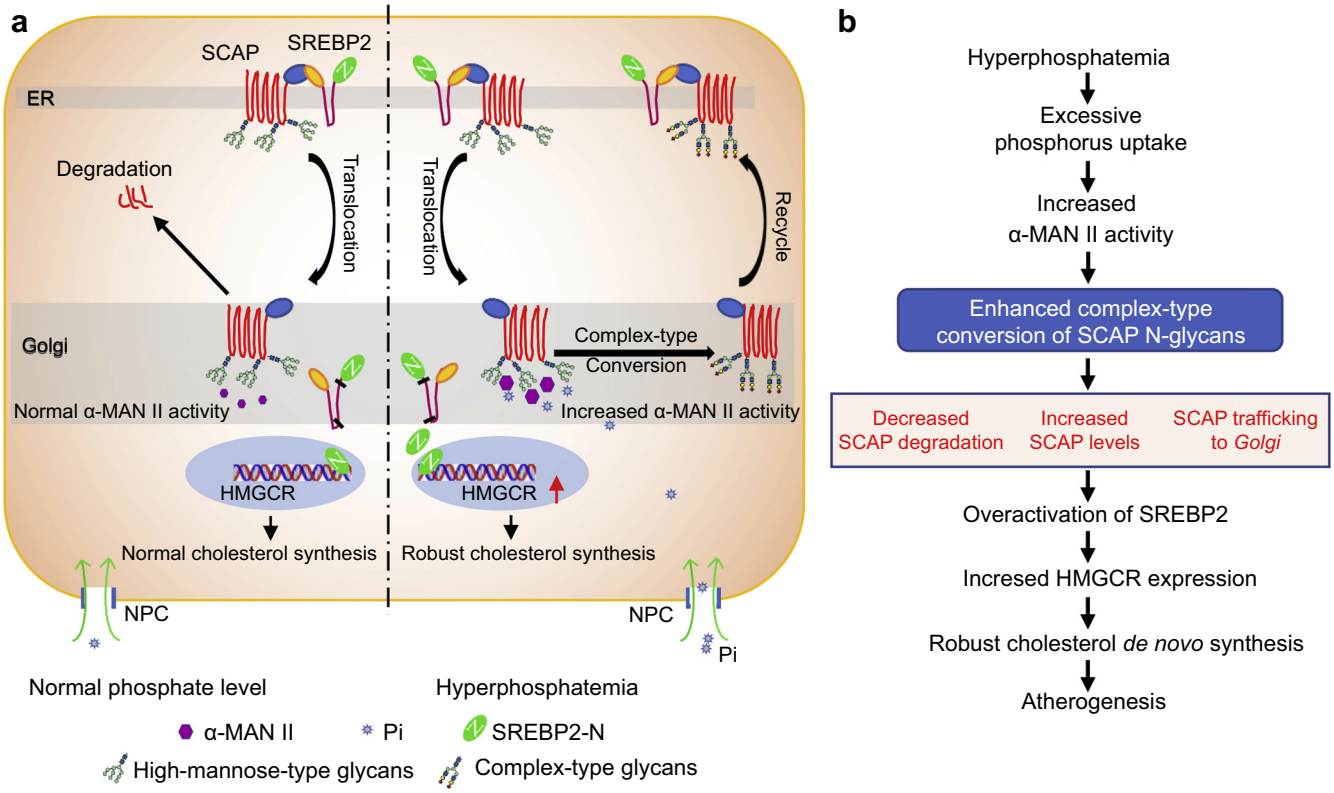

Figure 7 | Schematic diagram showing enhanced complex-type conversion of sterol regulatory element-binding protein (SREBP) cleavage-activating protein (SCAP) N-glycans by hyperphosphatemia via aberrant activation of α-mannosidase (α-MAN) II leading to robust cholesterol synthesis and atherogenesis. (**a**) Excess phosphate (Pi) enters vascular smooth muscle cells via the Na-Pi cotransporter (NPC) and enhances complex-type conversion of SCAP N-glycans by augmenting the activity of α-MAN II. As a result, the degradation of SCAP with complex glycans slows down, which recycles around the endoplasmic reticulum (ER) and Golgi and overactivates SREBP2, leading to robust cholesterol *de novo* synthesis, and thereby intracellular cholesterol accumulation and foam cell formation. (**b**) Signaling cascade for Pi uptake to complex-type conversion of SCAP N-glycans and robust cholesterol *de novo* synthesis. SREBP2-N, NH_2 terminal fragment of SREBP2.

of α-MAN II in raised phosphate conditions, indicating that α-MAN 2A1 and α-MAN 2A2 controlled complex-type conversion of SCAP N-glycans could be key factors for the pathogenesis of foam cell formation. Our findings further revealed that SCAP with complex-type glycans is more resistant to degradation than SCAP with high-mannose-type glycans (combining the results from Figure 4a, b, and f). A previous study demonstrated in glioblastoma cells that preventing N-glycosylation by glucose depletion accelerated the proteasome-dependent degradation of SCAP.[24] Our study suggested that not only N-glycosylation but the complex-type conversion of N-glycans by the α-MAN II could be decisive for the stability of SCAP. The best model to test the specific role of phosphate on lipid homeostasis is SCAP VSMCs knockout mice. However, SCAP is an essential molecule for the survival of eukaryotes. Both global and VSMC-specific SCAP knockout are lethal for mice. This is one limitation of this study.

Overall, our study demonstrated that excess phosphate enters VSMCs via sodium-dependent phosphate cotransporter and promotes the complex-type conversion of SCAP N-glycans by augmenting the activity of α-MAN II, which increases SCAP half-life and protein levels. As a result, SCAP with complex-type glycans recycle around the ER and Golgi and overactivate SREBP2, leading to robust *de novo* cholesterol synthesis and therefore intracellular cholesterol accumulation and foam cell formation (Figure 7). We provide a new view of a link between hyperphosphatemia and lipid metabolic disturbance, both of which are important risk factors for atherosclerosis. These findings may help our understanding of the pathogenesis of accelerated atherosclerosis and the high incidence of ASCVD in patients with CKD. It may also contribute to the design of effective dual therapeutic strategies targeting both phosphate and lipid metabolisms in the CKD population.

DISCLOSURE

All the authors declared no competing interests.

ACKNOWLEDGMENTS

This work was supported by National Key Research and Development (R&D) Program of China (grant 2018YFC1312700), National Natural Science Foundation of China (grants 81500341 and 32030054), Chongqing Science and Technology Commission (grants cstc2018jcyjAX0134, cstc2020jcyj-msxmX0304, and cstc2020jcyj-msxmX0152) and Moorhead Trust.

AUTHOR CONTRIBUTIONS

CZ, NOY, XZR, and QH contributed to the design of the study. CZ, NOY, TTZ, and QL conducted the experiments. HG, TTZ, and NOY collected the clinical data. CZ, TTZ, and NOY analyzed data. CZ, XZR, JFM, and ZV wrote the manuscript.

SUPPLEMENTARY MATERIAL

Supplementary File (Word)

Figure S1. Excess phosphate induced translocation of SCAP and cholesterol accumulation in THP-1 macrophages.

Figure S2. The dose response and time-course effect of excess phosphate on SCAP-SREBP2 signaling.

Table S1. The formula of the main nutrition grandients in normal chow and high-phosphate diet.

Table S2. Comparison of the basic characteristics between AS and non-AS groups.

Table S3. The univariate logistics regression analysis of vascular risk factors between AS and non-AS groups.

Table S4. Basic characteristics of normal chow– and high-phosphate diet–fed apoE$^{-/-}$ mice when sacrificed.

Table S5. Mouse TaqMan primers for real-time PCR.

Table S6. Human TaqMan primers for real-time PCR.

Supplementary References.

REFERENCES

1. GBD Chronic Kidney Disease Collaboration. Global, regional, and national burden of chronic kidney disease, 1990–2017: a systematic analysis for the Global Burden of Disease Study 2017. *Lancet*. 2020;395:709–733.
2. Reiss AB, Voloshyna I, De Leon J, et al. Cholesterol metabolism in CKD. *Am J Kidney Dis*. 2015;66:1071–1082.
3. Wanner C, Krane V, März W, et al. Atorvastatin in patients with type 2 diabetes mellitus undergoing hemodialysis. *N Engl J Med*. 2005;353:238–248.
4. Fellström BC, Jardine AG, Schmieder RE, et al. Rosuvastatin and cardiovascular events in patients undergoing hemodialysis. *N Engl J Med*. 2009;360:1395–1407.
5. Baigent C, Landray MJ, Reith C, et al. The effects of lowering LDL cholesterol with simvastatin plus ezetimibe in patients with chronic kidney disease (Study of Heart and Renal Protection): a randomised placebo-controlled trial. *Lancet*. 2011;377:2181–2192.
6. Michigami T, Kawai M, Yamazaki M, et al. Phosphate as a signaling molecule and its sensing mechanism. *Physiol Rev*. 2018;98:2317–2348.
7. Vervloet MG, Sezer S, Massy ZA, et al. The role of phosphate in kidney disease. *Nat Rev Nephrol*. 2017;13:27–38.
8. Yamada S, Giachelli CM. Vascular calcification in CKD-MBD: roles for phosphate, FGF23, and Klotho. *Bone*. 2017;100:87–93.
9. Vervloet MG, van Ballegooijen AJ. Prevention and treatment of hyperphosphatemia in chronic kidney disease. *Kidney Int*. 2018;93:1060–1072.
10. Foley RN, Collins AJ, Herzog CA, et al. Serum phosphorus levels associate with coronary atherosclerosis in young adults. *J Am Soc Nephrol*. 2009;20:397–404.
11. Dhingra R, Sullivan LM, Fox CS, et al. Relations of serum phosphorus and calcium levels to the incidence of cardiovascular disease in the community. *Arch Intern Med*. 2007;167, 879–855.
12. Narang R, Ridout D, Nonis C, et al. Serum calcium, phosphorus and albumin levels in relation to the angiographic severity of coronary artery disease. *Int J Cardiol*. 1997;60:73–79.
13. Ellam T, Wilkie M, Chamberlain J, et al. Dietary phosphate modulates atherogenesis and insulin resistance in apolipoprotein E knockout mice-brief report. *Arterioscler Thromb Vasc Biol*. 2011;31:1988–1990.
14. Phan O, Ivanovski O, Nguyen-Khoa T, et al. Sevelamer prevents uremia-enhanced atherosclerosis progression in apolipoprotein E-deficient mice. *Circulation*. 2005;112:2875–2882.
15. Nikolov IG, Joki N, Nguyen-Khoa T, et al. Lanthanum carbonate, like sevelamer-HCL, retards the progression of vascular calcification and atherosclerosis in uremic apolipoprotein E-deficient mice. *Nephrol Dial Transplant*. 2012;27:505–513.
16. Ellam TJ, Chico TJ. Phosphate: the new cholesterol? The role of the phosphate axis in non-uremic vascular disease. *Atherosclerosis*. 2012;220:310–318.
17. Tanaka S, Yamamoto H, Nakahashi O, et al. Dietary phosphate restriction induces hepatic lipid accumulation through dysregulation of cholesterol metabolism in mice. *Nutr Res*. 2013;33:586–593.
18. Shao W, Espenshade PJ. Expanding roles for SREBP in metabolism. *Cell Metab*. 2012;16:414–419.
19. Kuan YC, Takahashi Y, Maruyama T, et al. Ring finger protein 5 activates sterol regulatory element-binding protein 2 (SREBP2) to promote cholesterol biosynthesis via ubiquitinating SREBP chaperone SCAP. *J Biol Chem*. 2020;295:3918–3928.
20. Brown MS, Radhakrishnan A, Goldstein JL. Retrospective on cholesterol homeostasis: the central role of Scap. *Annu Rev Biochem*. 2018;87:783–807.
21. Gao Y, Zhou Y, Goldstein JL, et al. Cholesterol-induced conformational changes in the sterol-sensing domain of the Scap protein suggest feedback mechanism to control cholesterol synthesis. *J Biol Chem*. 2017;292:8729–8737.
22. Nohturfft A, DeBose-Boyd RA, Scheek S, et al. Sterols regulate cycling of SREBP cleavage-activating protein (SCAP) between endoplasmic reticulum and Golgi. *Proc Natl Acad Sci U S A*. 1999;96:11235–11240.
23. Shao W, Espenshade PJ. Sterol regulatory element-binding protein (SREBP) cleavage regulates Golgi-to-endoplasmic reticulum recycling of SREBP cleavage-activating protein (SCAP). *J Biol Chem*. 2014;289:7547–7557.
24. Cheng C, Ru P, Geng F, et al. Glucose-mediated N-glycosylation of SCAP is essential for SREBP-1 activation and tumor growth. *Cancer Cell*. 2015;28:569–581.
25. Chen Y, Ku H, Zhao L, et al. Inflammatory stress induces statin resistance by disrupting 3-hydroxy-3-methylglutaryl-CoA reductase feedback regulation. *Arterioscler Thromb Vasc Biol*. 2014;34:365–376.
26. Yuan Y, Zhao L, Chen Y, et al. Advanced glycation end products (AGEs) increase human mesangial foam cell formation by increasing Golgi SCAP glycosylation in vitro. *Am J Physiol Renal Physiol*. 2011;301:F236–F243.
27. Li D, Chen A, Lan T, et al. SCAP knockdown in vascular smooth muscle cells alleviates atherosclerosis plaque formation via up-regulating autophagy in ApoE-/- mice. *FASEB J*. 2019;33:3437–3450.
28. Ruan XZ, Varghese Z, Powis SH, et al. Dysregulation of LDL receptor under the influence of inflammatory cytokines: a new pathway for foam cell formation. *Kidney Int*. 2001;60:1716–1725.
29. Ma KL, Ruan XZ, Powis SH, et al. Inflammatory stress exacerbates lipid accumulation in hepatic cells and fatty livers of apolipoprotein E knockout mice. *Hepatology*. 2008;48:770–781.
30. Jono S, McKee MD, Murry CE, et al. Phosphate regulation of vascular smooth muscle cell calcification. *Circ Res*. 2000;87:E10–E17.
31. Nohturfft A, Brown MS, Goldstein JL. Topology of SREBP cleavage-activating protein, a polytopic membrane protein with a sterol-sensing domain. *J Biol Chem*. 1998;273:17243–17250.
32. Daniel PF, Winchester B, Warren CD. Mammalian alpha-mannosidases—multiple forms but a common purpose? *Glycobiology*. 1994;4:551–566.
33. Moremen KW. Golgi alpha-mannosidase II deficiency in vertebrate systems: implications for asparagine-linked oligosaccharide processing in mammals. *Biochim Biophys Acta*. 2002;1573:225–235.
34. Di Marco GS, König M, Stock C, et al. High phosphate directly affects endothelial function by downregulating annexin II. *Kidney Int*. 2013;83:213–222.
35. Ruan XZ, Varghese Z, Moorhead JF. An update on the lipid nephrotoxicity hypothesis. *Nat Rev Nephrol*. 2009;5:713–721.
36. Smirnov AN. Lipid signaling in the atherogenesis context. *Biochemistry (Mosc)*. 2010;75:793–810.
37. Sakai K, Nagashima S, Wakabayashi T, et al. Myeloid HMG-CoA (3-hydroxy-3-methylglutaryl-coenzyme A) reductase determines atherosclerosis by modulating migration of macrophages. *Arterioscler Thromb Vasc Biol*. 2018;38:2590–2600.
38. Hwang S, Hartman IZ, Calhoun LN, et al. Contribution of accelerated degradation to feedback regulation of 3-hydroxy-3-methylglutaryl coenzyme A reductase and cholesterol metabolism in the liver. *J Biol Chem*. 2016;291:13479–13494.
39. Zhang X, Wang Y. Glycosylation quality control by the Golgi structure. *J Mol Biol*. 2016;428:3183–3193.
40. Kornfeld R, Kornfeld S. Assembly of asparagine-linked oligosaccharides. *Annu Rev Biochem*. 1985;54:631–664.
41. Moremen KW, Tiemeyer M, Nairn AV. Vertebrate protein glycosylation: diversity, synthesis and function. *Nat Rev Mol Cell Biol*. 2012;13:448–462.